Supplement of Atmos. Chem. Phys., 24, 6937–6963, 2024
https://doi.org/10.5194/acp-24-6937-2024-supplement

Atmospheric Chemistry and Physics
Open Access
EGU

Supplement of

California wildfire smoke contributes to a positive atmospheric temperature anomaly over the western United States

James L. Gomez et al.

Correspondence to: James L. Gomez (jgome222@ucr.edu)

S1 Additional Method Verification with Correlations

The methods for this paper were employed as typical cross correlations would not be able to differentiate effects of fires from fire weather, and on a daily scale cross correlations are not possible due to missing data. However, the results of the double stratification should be reflected in monthly cross correlation between nCA DM and the variables of interest. Figure 13 was replicated with the monthly cross correlation method. This yielded results consistent with the methods utilized in this paper (Figure S2). Figure S2 showcases that the warming of the cloud layer and corresponding reduction in RH and CF are comparable spatially to that of Figure 13 and Figure S11. Consistency between the stratification method as well as the monthly cross correlation method indicate that the temporal error introduced by using GFED DM is in fact negligible, and that the method utilized in this paper is sound.

S2 CALIPSO

The CALIPSO satellite dataset utilized is the AL_LID_L3_Tropospheric_APro_AllSky-Standard-V4-20 dataset (Tackett et al., 2018; Winker, 2019). CALIPSO was utilized to confirm that the large fires are associated with an increase in extinction coefficient EC of aerosols, and which atmospheric layers the largest increases in absorbing aerosols are observed. While all other data sets in this study are daily data, CALIPSO only has monthly data available, and this data is at a much coarser resolution (2^o latitude x 5^o longitude). Additionally, CALIPSO only has available data between 2006-2021, while all other utilized datasets have data available from 2003-2022 for the relevant seasonal time period. For level 3 EC data, CALIPSO distinguishes between 3 types of aerosol: dust, polluted dust, and smoke. Since CALIPSO data is not temporally consistent with the other data products utilized in this paper, it is only used for comparison for MERRA-2 aerosol profiles in this supplement.

S2.1 CALIPSO Profiles

To determine the difference in EC profile between anomalously high and low fire events, the average for each aerosol type's monthly EC anomaly at each pressure level was taken over ($DM90$) months and ($DM10$) months in the 2006-2021 range (the time period in which CALIPSO data is available) in the region of interest. The difference between these two profiles is then taken. The motivation for this process is for one to remove the effects of potential background aerosols such as BC or OA (from anthropogenic sources such as fossil fuel burning) and isolate the effects of the aerosols emitted from mega-fires. The resulting profile then depicts the effects on the vertical EC profile that fires have. The EC profile of the aerosols is not further stratified as the CALIPSO data is monthly.

The three absorbing aerosols that are associated with fires that can be discerned by CALIPSO are smoke, dust, and polluted dust. However, increases in non-polluted dust during fires may be related to the concurrence of high winds that tend to be a driver of the large fires themselves. Emissions of polluted dust, however, are far more likely to be related to fires, as this aerosol species is a combination of dust and smokey aerosols. Therefore, focus was placed upon smoke and polluted dust. Polluted dust is a mixture of smoke and dust, and therefore should have stronger SW absorption than dust alone. Polluted dust is classified as a combination of wind-blown dust from the AERONET coarse dust clusters and fine biomass burning aerosols clusters (Omar et al., 2009). Figure S7 depicts monthly 2006-2021 nCA-NV regional average $EC(DM90)$-$EC(DM10)$ in the daytime (Figure S7a) and the nighttime (Figure S7b) for both smoke and polluted dust. These plots demonstrate that polluted dust and smoke EC increases significantly in most parts of the troposphere in months where an anomalously large fire occurs. This includes altitudes with pressures p less than 500 hPa, where there are relatively large and significant increases in polluted dust (Figure S7c,d).

S3 Changes in Circulation

S3.1 MERRA-2 Wind and Pressure Velocity Product

The MERRA-2 3-hourly reanalysis dataset (Global Modeling And Assimilation Office and Pawson, 2015) (M2I3NPASM) was used to analyze profiles of vertical pressure velocity Ω as well as both eastern and northern wind speed.

S3.2 Changes in Wind Vectors

In Figure 9d-f, it is noted that there is a significant decrease in M_{H_2O} in the cloud layer over northern Nevada. Therefore, it appears possible that there is moisture advection from northern Nevada to elsewhere. Figure S9 depicts MERRA-2 wind vector and wind speed anomalies in the cloud layer for high compared to low DM days under simultaneously high and low RH_s anomaly conditions. There is a clockwise anti-cyclonic anomaly over the region under both RH_s conditions that is consistent with Santa Ana wind events (Keeley and Syphard, 2019). However, the Santa Ana wind conditions do not appear to be robustly stronger in either scenario, as very few significant positive wind speed anomalies exist. However, there is a positive and significant wind speed anomaly in northeastern Nevada that corresponds with a decrease in water mass mixing ratio Figure S9b under high RH_s conditions. If moisture advection were occurring in this region, due to the cyclonic flow it would likely be carried towards southern Nevada and southern California, where significant positive water mass mixing ratio anomalies exist Figure S9b. This implies that part of the decrease in RH and CF_{cir} over northern Nevada could be due to a difference in the strength of the Santa Ana wind event in northeastern Nevada that transports moisture elsewhere. It is unknown if this change in wind speed is due to the T anomalies in the region, or if these wind patterns are an artifact that was not filtered out from analyzing high RH_s conditions. However, further analysis of moisture flux convergence and geopotential height anomalies is required to make solid conclusions.

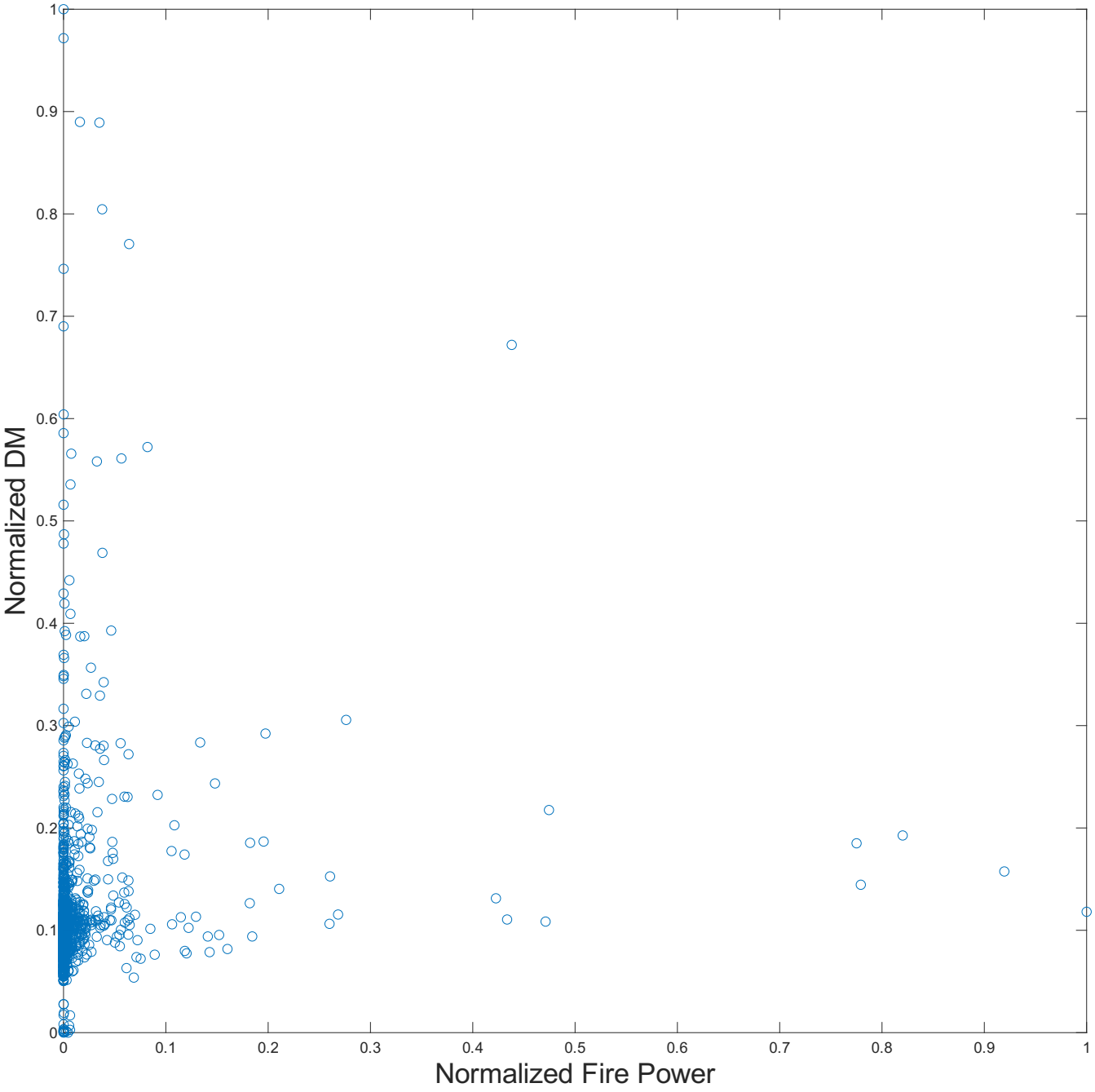

Figure S1. Normalized daily Global Fire Emission Database v4 dry matter emissions DM vs normalized daily MODIS Aqua fire power (FP) in northern California. Data consists of all available days within 2003-2022 fire seasons for both datasets. If using each variable as a metric of fire emission, MODIS Aqua FP systematically underestimates days of high fire emission relative to GFED DM. This is likely due to cloud cover obstructing daily FP retrievals in MODIS, and due to vegetation type being important for fire emission estimation.

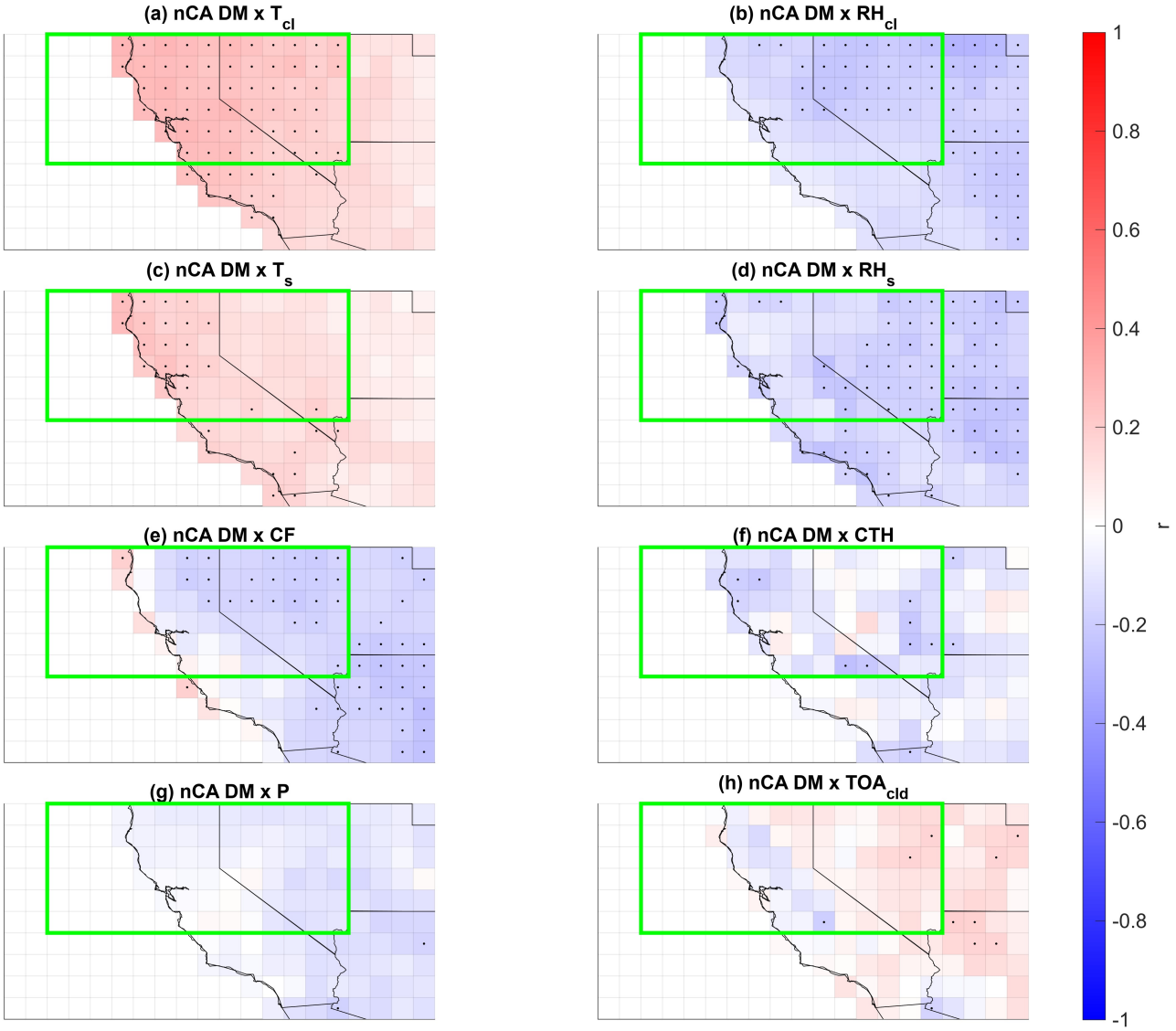

Figure S2. 2003-2022 June-October (fire season) monthly cross correlations between northern California (nCA) regional average wildfire dry matter emissions DM and the meteorological variables. Includes (a) cloud layer (850-300 hPa) temperature T, (b) cloud layer relative humidity RH, surface temperature T_s, surface relative humidity RH_s, cloud fraction CF, cloud top height CTH, precipitation P, and outgoing top of atmosphere shortwave radiation TOA. Black dots represent statistically significant cross correlation values at the 90% confidence interval using a two-tailed test.

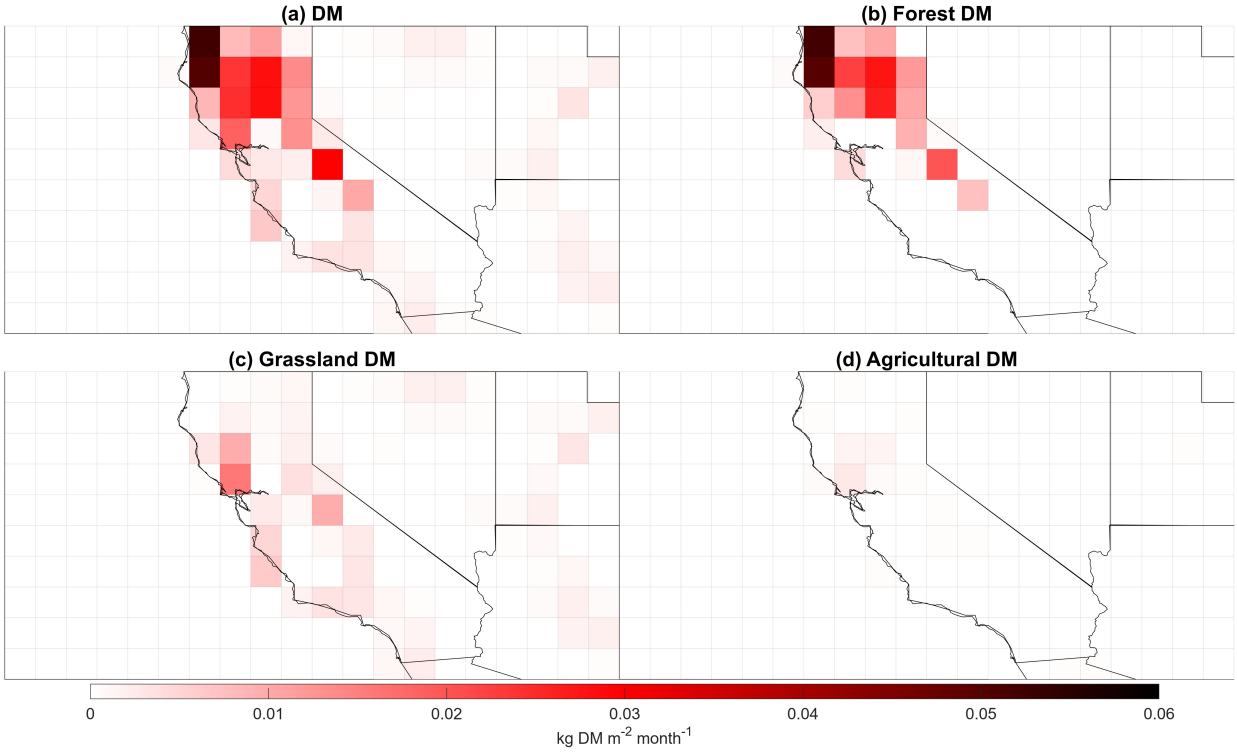

Figure S3. 20-year seasonal average fire dry matter (DM) emissions per biome over the south western US. 2003-2022 June-October seasonal average DM emissions for (a) all biomes, (b) temperate forests, (c) grasslands, and (d) agricultural land. The majority of dry matter emissions come from temperate forests, followed by grasslands, then agricultural lands contribute minimally to net DM emissions.

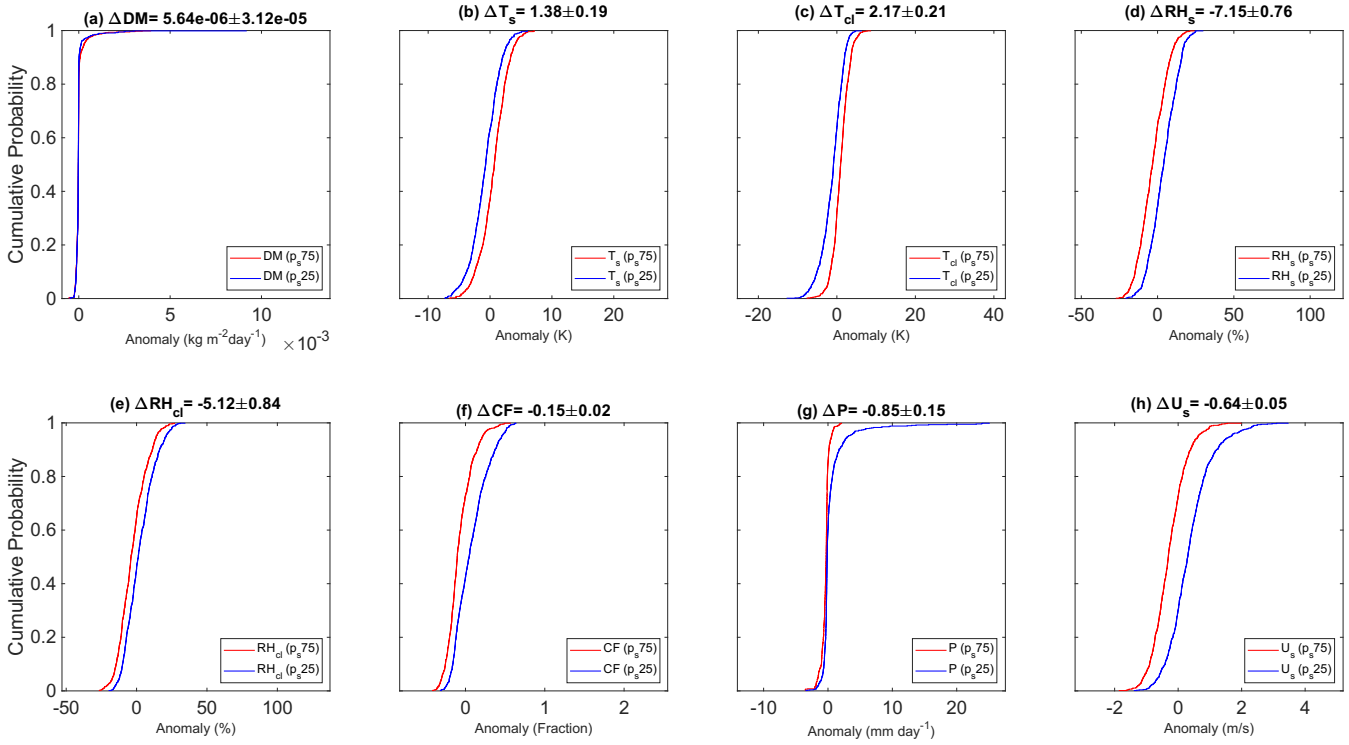

Figure S4. Dependence of meteorological variables on high versus low surface pressure p_s during the fire season. Regional average cumulative distribution functions (CDFs) for variable anomalies stratified by 75th percentile surface pressure (p_s75) days (red) and 25th percentile (p_s25) (blue) days within the 2003-2022 June-October time period. Variables depicted include (a) northern California (nCA) fire dry matter (DM) emissions, (b) northern California-Nevada (nCA-NV) surface temperature T_s, (c) nCA-NV cloud layer (850-300 hPa) average temperature T_{cl} , (d) nCA-NV surface relative humidity RH_s, (e) nCA-NV cloud layer average relative humidity RH_{cl} , (f) nCA-NV cloud fraction CF, (g) nCA-NV precipitation P, and (h) nCA-NV surface wind speed U_s. Δ represents the difference between the variable's average anomaly for p_s75 and p_s25 days.

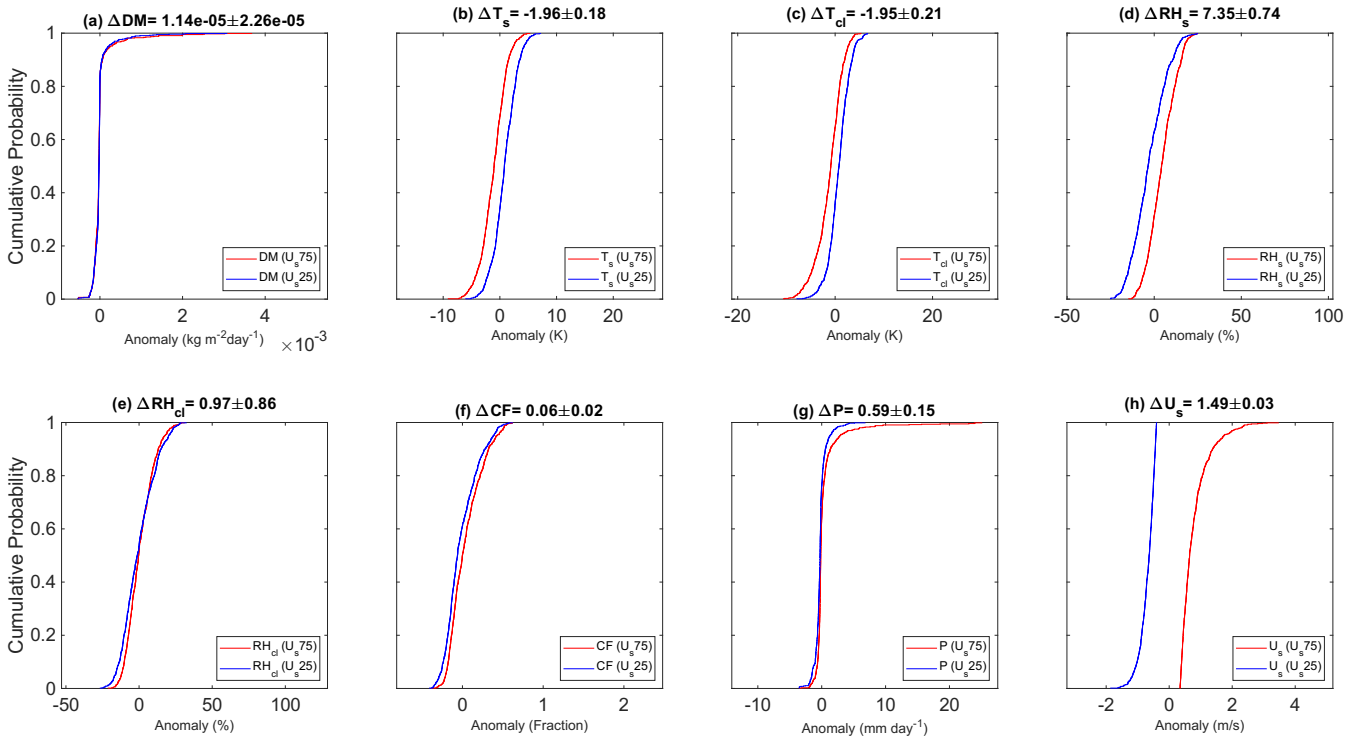

Figure S5. Dependence of meteorological variables on high versus low surface wind U_s during the fire season. Regional average cumulative distribution functions (CDFs) for variable anomalies stratified by 75th percentile surface wind (U_s75) days (red) and 25th percentile (U_s25) (blue) days within the 2003-2022 June-October time period. Variables depicted include (a) northern California (nCA) fire dry matter (DM) emissions, (b) northern California-Nevada (nCA-NV) surface temperature T_s, (c) nCA-NV cloud layer (850-300 hPa) average temperature T_{cl} , (d) nCA-NV surface relative humidity RH_s, (e) nCA-NV cloud layer average relative humidity RH_{cl} , (f) nCA-NV cloud fraction CF, (g) nCA-NV precipitation P, and (h) nCA-NV surface wind speed U_s. Δ represents the difference between the variable's average anomaly for U_s75 and U_s25 days.

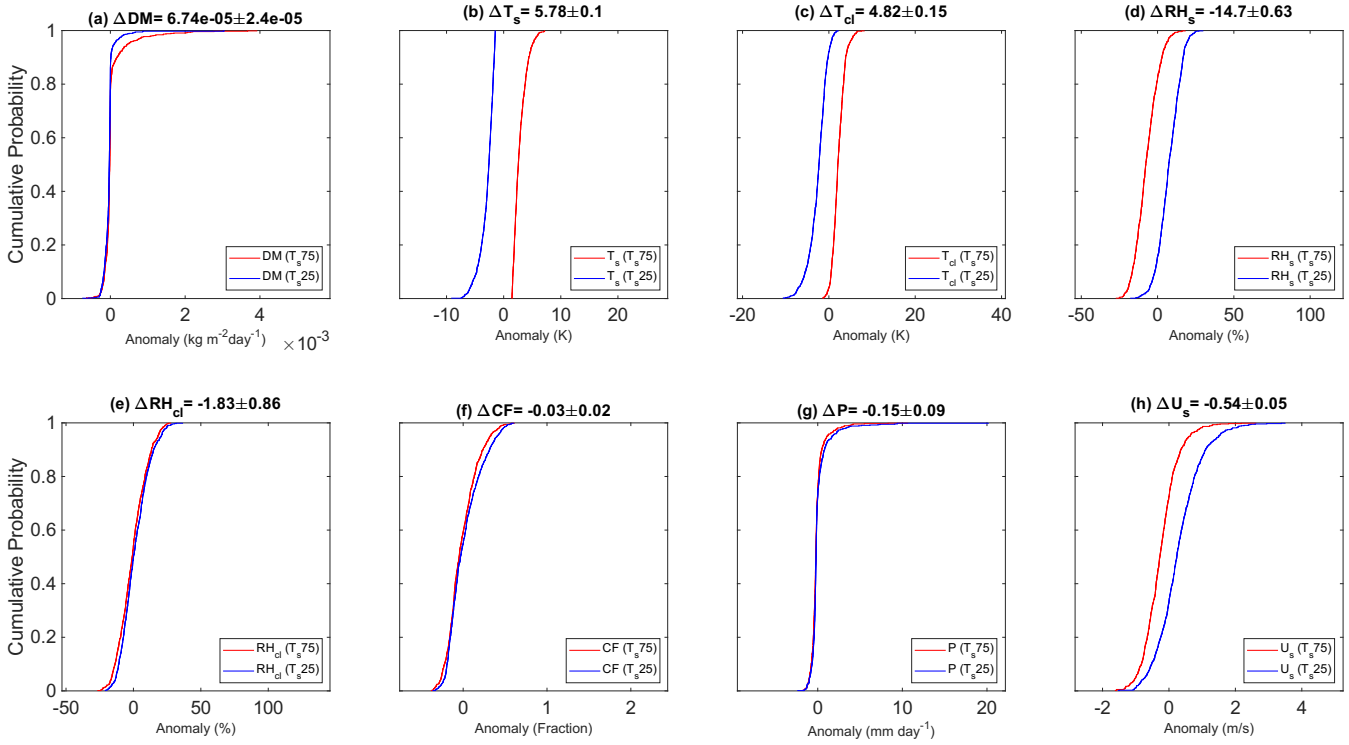

Figure S6. Dependence of meteorological variables on high versus low surface temperature T_s during the fire season. Regional average cumulative distribution functions (CDFs) for variable anomalies stratified by 75th percentile surface temperature (T_s75) days (red) and 25th percentile (T_s25) (blue) days within the 2003-2022 June-October time period. Variables depicted include (a) northern California (nCA) fire dry matter (DM) emissions, (b) northern California-Nevada (nCA-NV) surface temperature T_s, (c) nCA-NV cloud layer (850-300 hPa) average temperature T_{cl} , (d) nCA-NV surface relative humidity RH_s, (e) nCA-NV cloud layer average relative humidity RH_{cl} , (f) nCA-NV cloud fraction CF, (g) nCA-NV precipitation P, and (h) nCA-NV surface wind speed U. Δ represents the difference between the variable's average anomaly for T_s75 and T_s25 days.

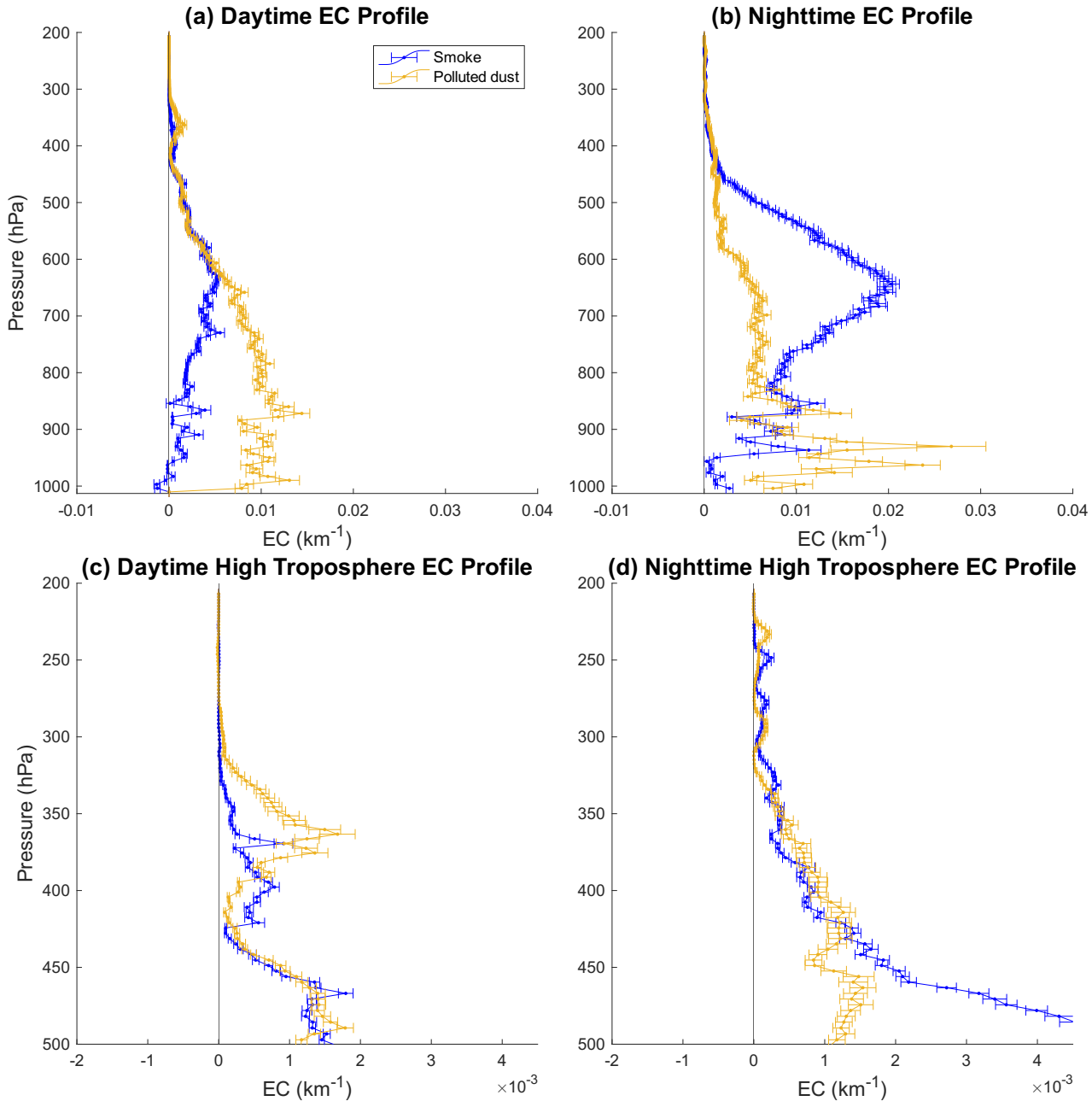

Figure S7. Aerosols extinction coefficient EC anomaly profiles on high minus low fire months during the fire season. Difference in 2006-2021 northern California/Nevada (nCA-NV) regional average CALIPSO EC profiles that occur in 90th percentile northern California (nCA) fire emission months and 10th percentile nCA fire emission months within the 2006-2021 June-October time period. Blue represents the smoke EC profile, and gold represents the polluted dust EC profile. (a,c) depict the daytime CALIPSO retrievals, while (b,d) depict nighttime CALIPSO retrievals. (a) and (b) display the entire vertical EC profiles, while (c,d) display the profiles in the high troposphere (pressures less than 500 hPa). Error bars represent the 90% confidence interval.

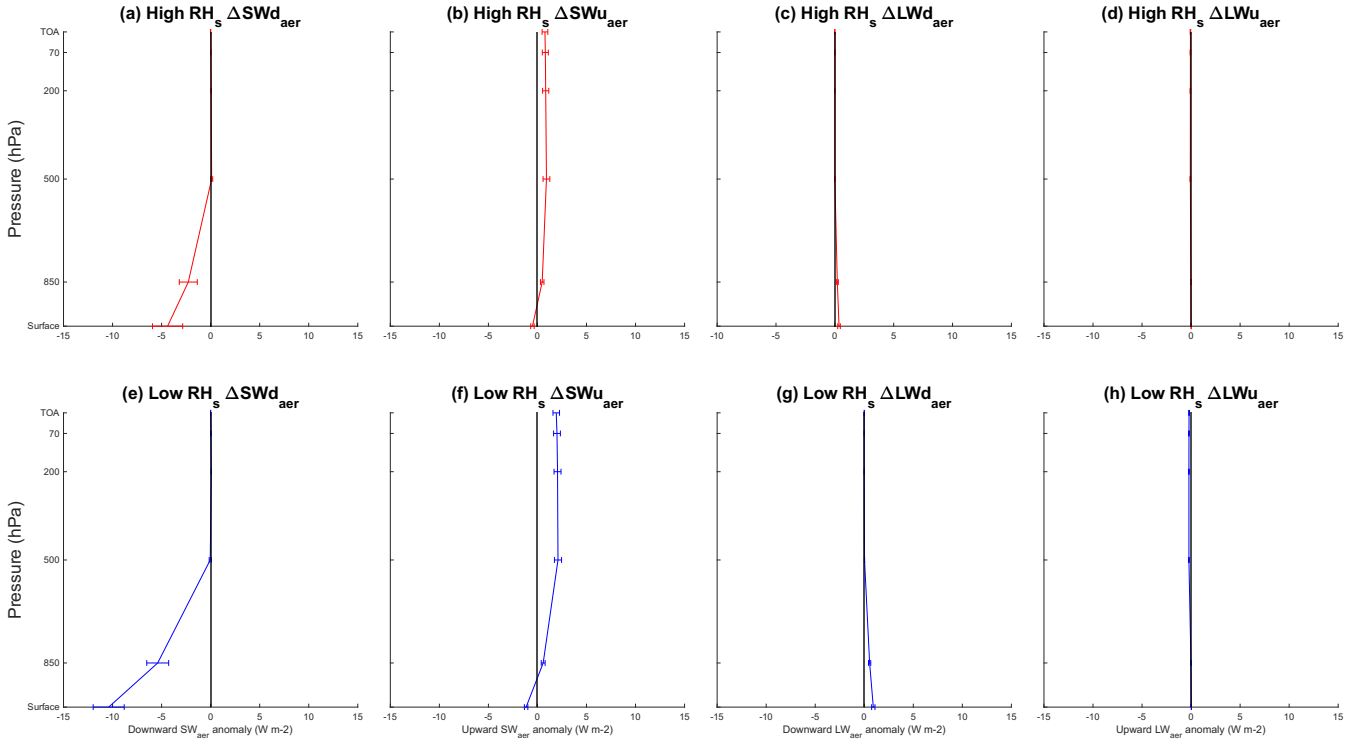

Figure S8. Aerosol-only (all-sky minus no aerosol) atmospheric CERES radiative flux profiles in the 2003-2022 June-October time period. High minus low fire condition CERES radiative flux profiles stratified by (a-d) high RH_s and (e-h) low RH_s conditions for (a,e) downward shortwave flux SWd, (b,f) upward shortwave flux SWu, (c,g) downward longwave flux LWd , and (d,h) upward longwave flux LWu. Error bars represent 90% confidence interval.

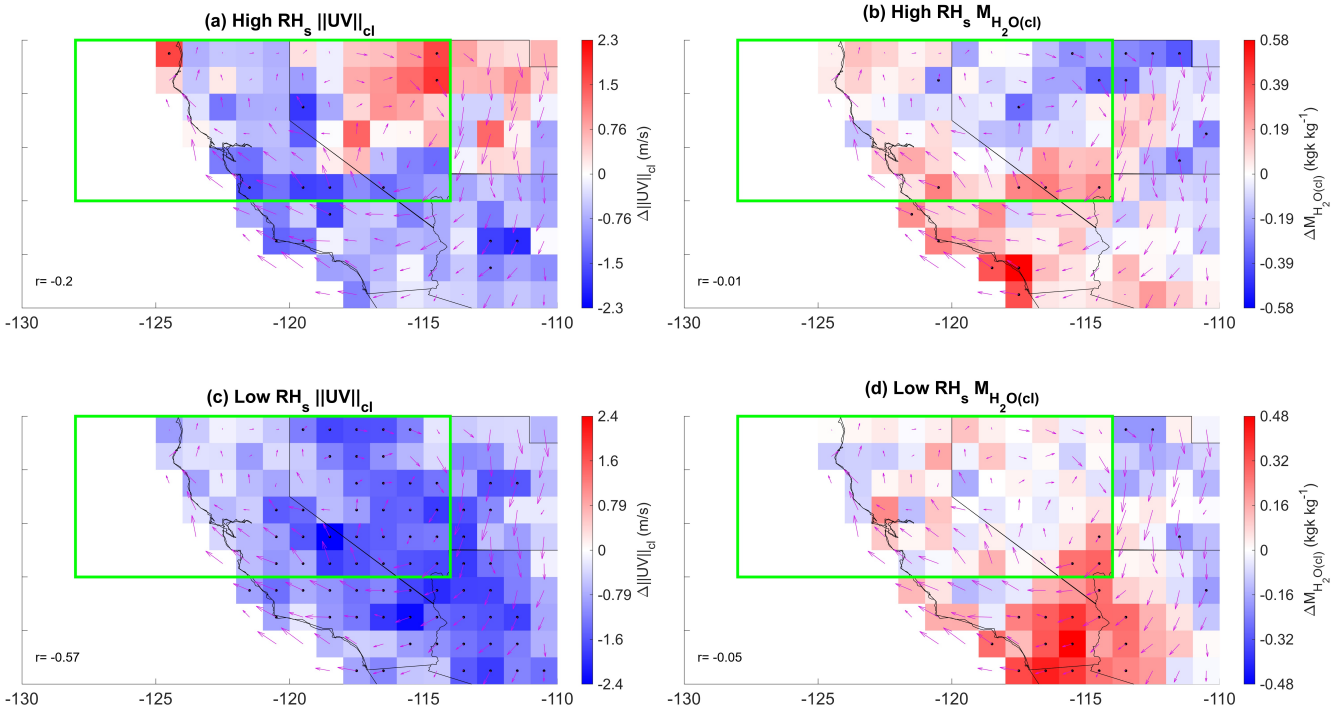

Figure S9. Fire effect (high minus low DM anomaly) on 850 hPa-300 hPa wind anomalies under differing RH_s conditions in the 2003-2022 June-October time period. Fire season high (90th percentile) minus low (10th percentile) nCA DM anomaly days cloud layer (a,c) northeastern wind speed magnitude $||UV||_{cl}$ anomalies and (b,d) water mass mixing ratio $M_{H_2O(cl)}$, under high RH_s (a,b) as well as low RH_s (c,d) conditions. Length of vectors and the color of grid cell represent magnitude of wind speed anomalies. Arrows represent wind vector anomalies. Black dots represent statistically significant differences at the 90% confidence interval. r-values represent correlations between the variable of interest and AOD.

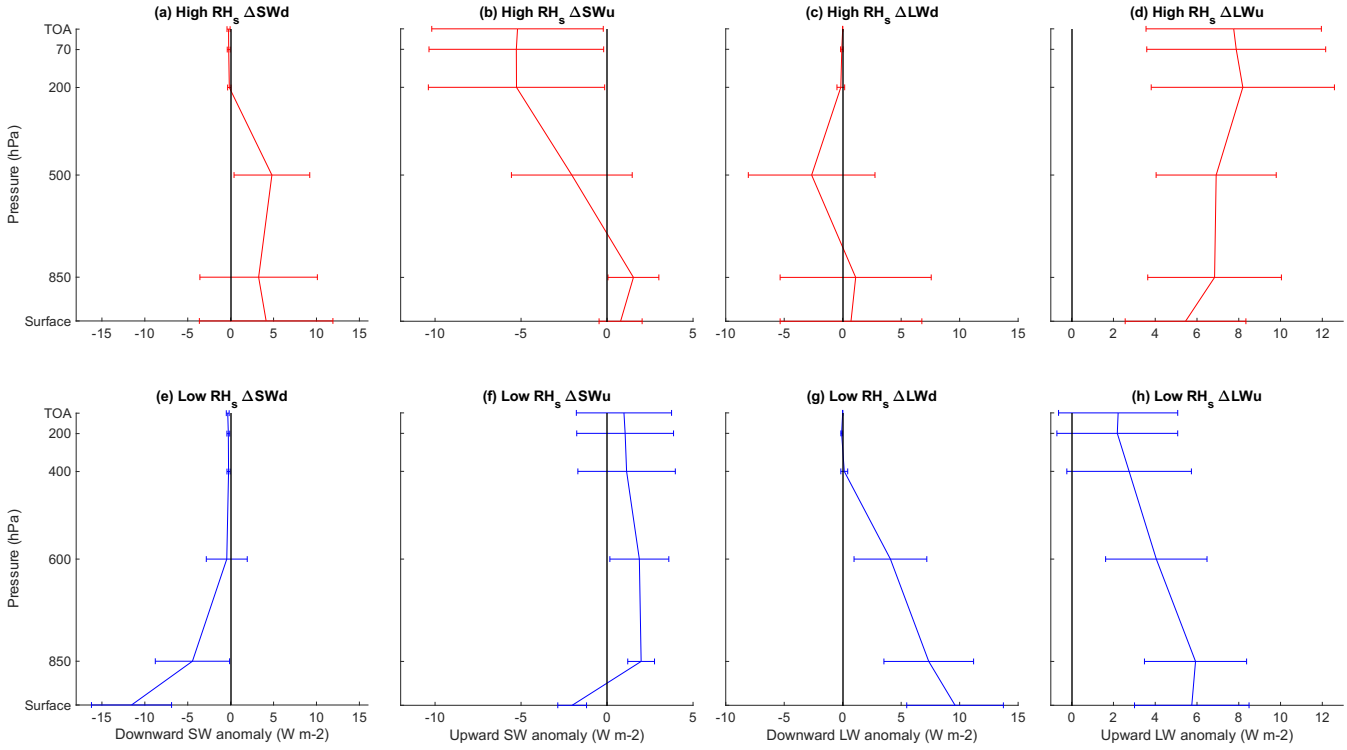

Figure S10. Fire effect on total atmospheric CERES radiative flux profiles in the 2003-2022 June-October time period. Fire effect CERES radiative flux profiles stratified by (a-d) high RH_s and (e-h) low RH_s conditions for (a,e) SWd, (b,f) SWu, (c,g) LWd, and (d,h) LWu. Error bars represent 90% confidence interval.

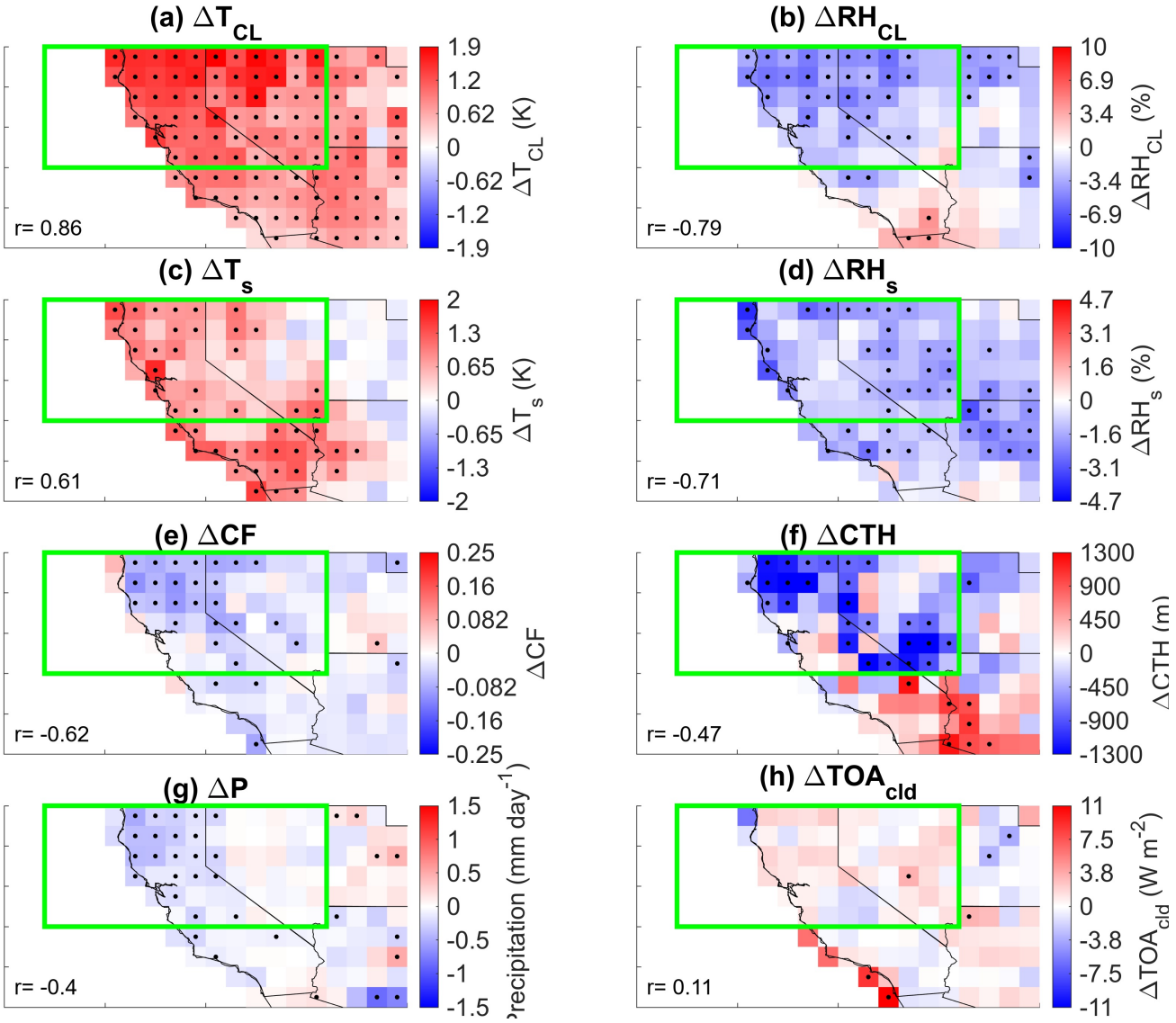

Figure S11. Meteorological responses under high versus low fire days with simultaneously low RH_s during the fire season. Difference between average variable anomalies on high nCA fire dry matter DM emission days and low nCA DM emission days that occur on low nCA-NV RH_s days in the 2003-2022 June-October time period. Variables include (a) 850 hPa-300 hPa average Temperature T_{cl}, 850 hPa-300 hPa average relative humidity RH_{cl}, (c) surface temperature T_s, (d) surface relative humidity RH_s, (e) cloud fraction CF, (f) cloud top height CTH, (g) precipitation P, and (e) top of atmosphere TOA shortwave cloud-only SW flux. Black dots represent statistically significant differences at the 90% confidence interval according to a two tailed test. Pearson cross correlation r values in each plot represent the spatial correlation between MODIS AOD anomaly and the variable anomaly depicted in the figure.

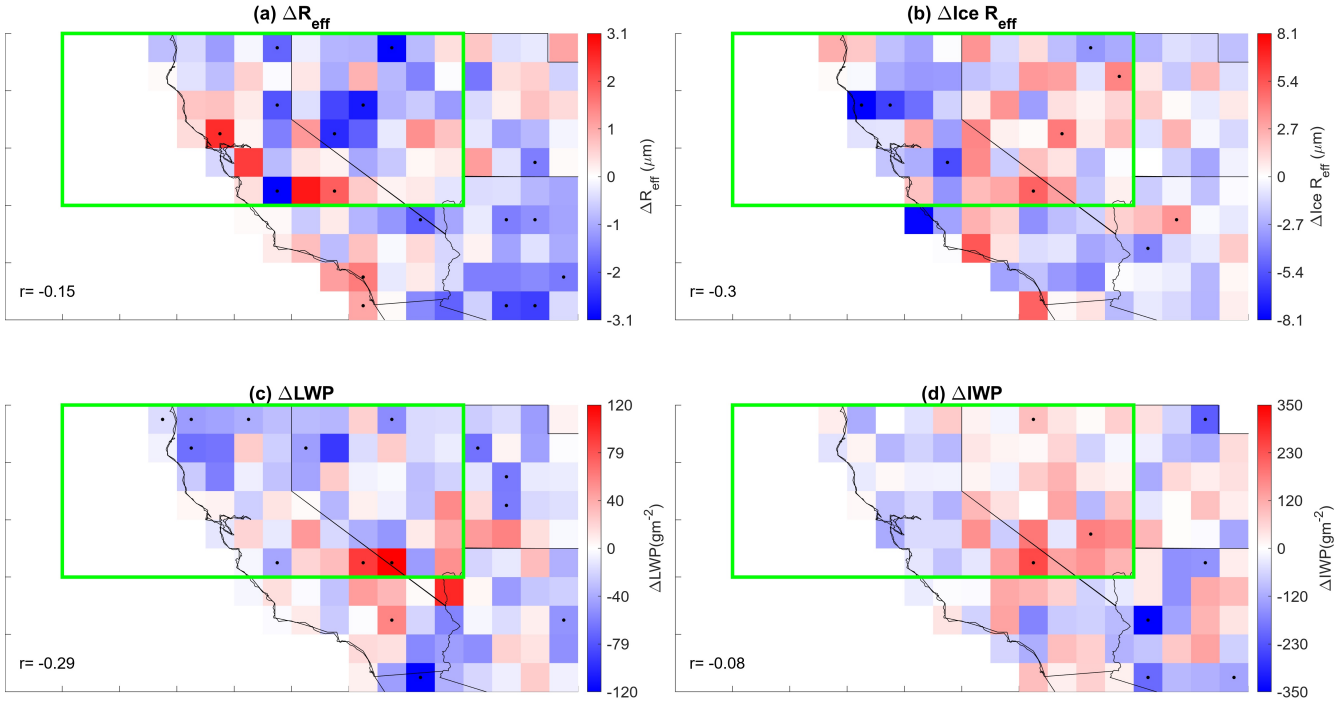

Figure S12. Cloud microphysical responses under high versus low fire days with simultaneously high RH_s in the 2003-2022 June-October time period. Difference between temporal average variable anomalies on high (90th percentile) northern California (nCA) fire dry matter DM emission days and low (10th percentile) nCA DM emission days that occur on high RH_s days. Variables include (a) liquid water effective radius R_{eff}, (b) ice R_{eff}, (c) liquid water path LWP, and (d) ice water path IWP. Black dots represent statistically significant differences. r represents Pearson cross correlation coefficient values for cross correlations between aerosol optical depth and the variable of interest.

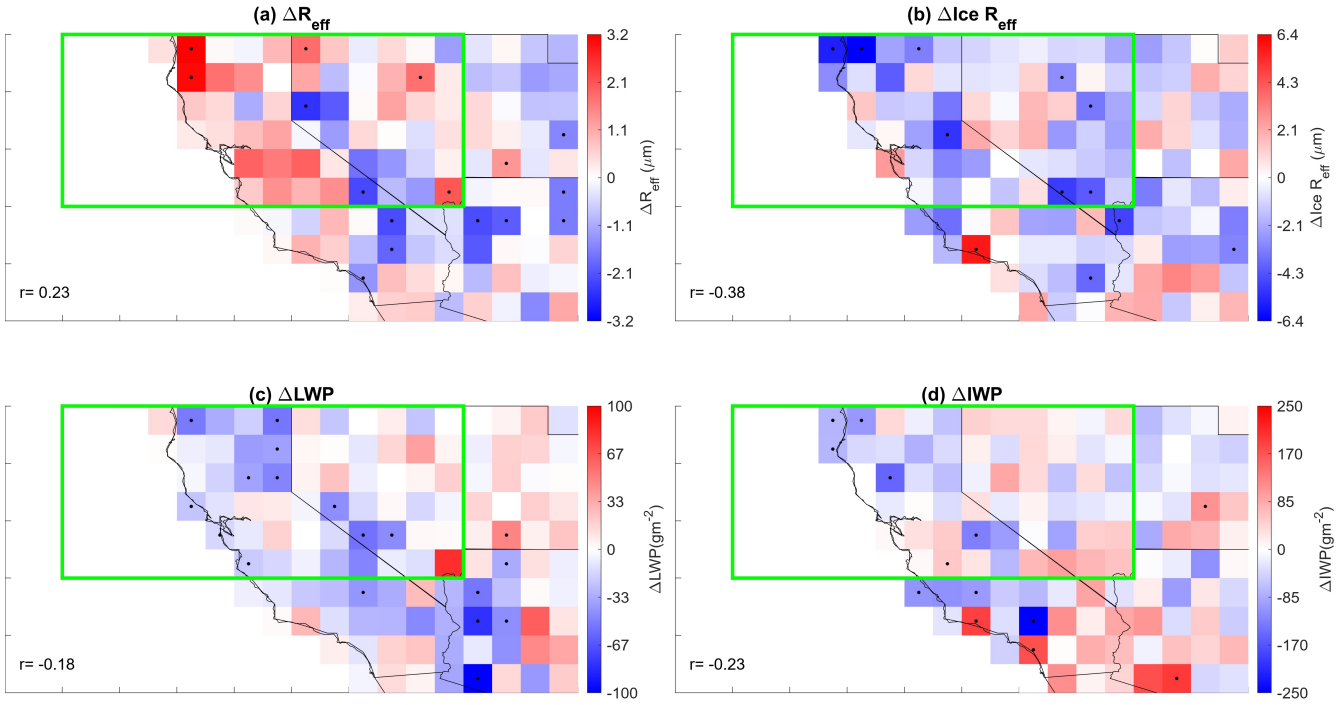

Figure S13. Cloud microphysical responses under high versus low fire days with simultaneously low RH_s in the 2003-2022 June-October time period. Difference between temporal average variable anomalies on high (90th percentile) northern California (nCA) fire dry matter DM emission days and low (10th percentile) nCA DM emission days that occur on high RH_s days. Variables include (a) liquid water effective radius R_{eff}, (b) ice R_{eff}, (c) liquid water path LWP, and (d) ice water path IWP. Black dots represent statistically significant differences. The green rectangle represents the northern California-Nevada region. r represents Pearson cross correlation coefficient values for cross correlations between aerosol optical depth and the variable of interest.

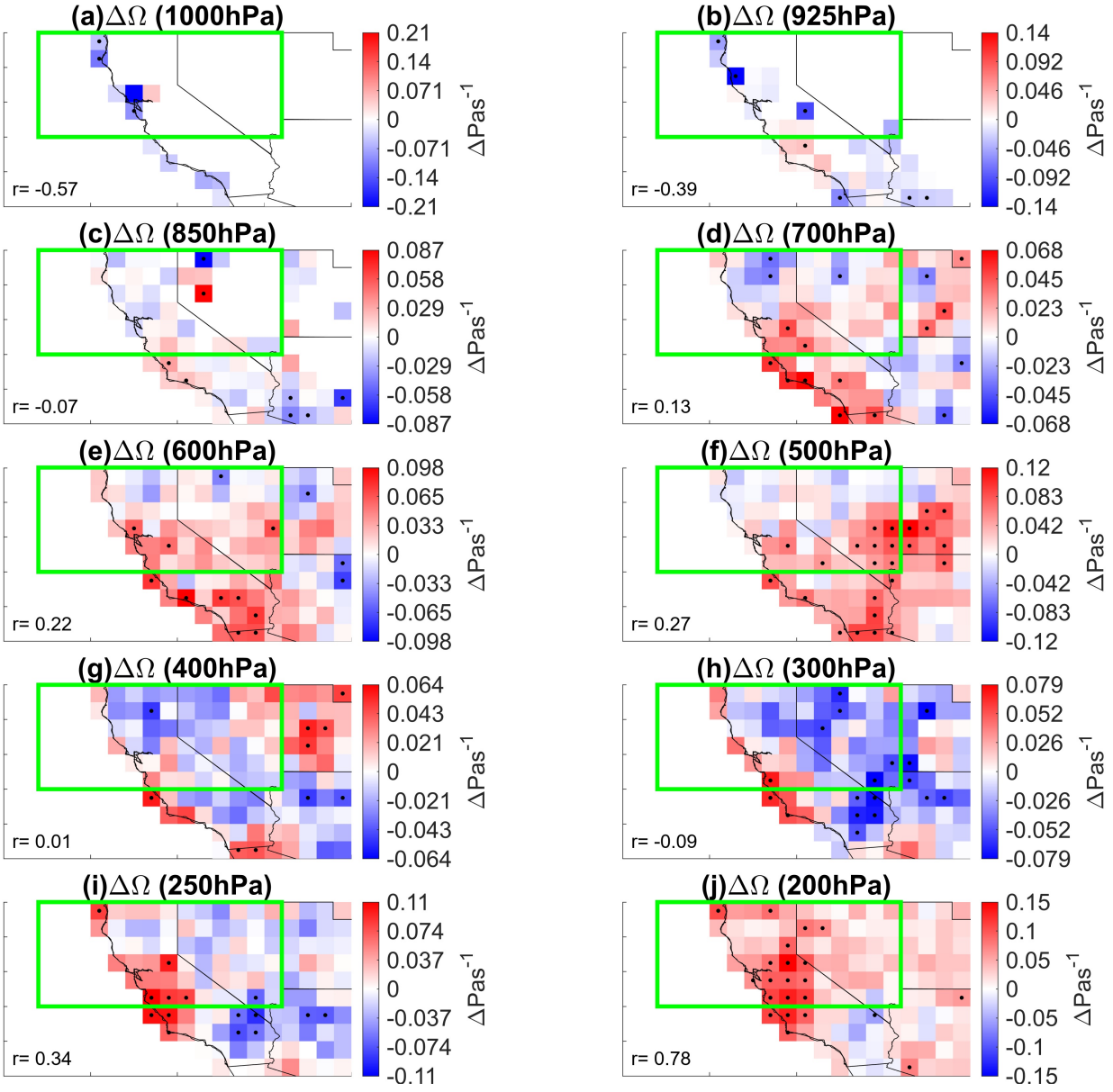

Figure S14. High minus low DM days' MERRA-2 Ω anomalies at all AIRS pressure levels from 1000 hPa to 200 hPa (a-j) under low RH_s conditions in the 2003-2022 June-October time period. Black dots indicate statistical significance at the 90% confidence interval. r values indicate spatial Pearson cross correlations between total Ω and MODIS AOD.

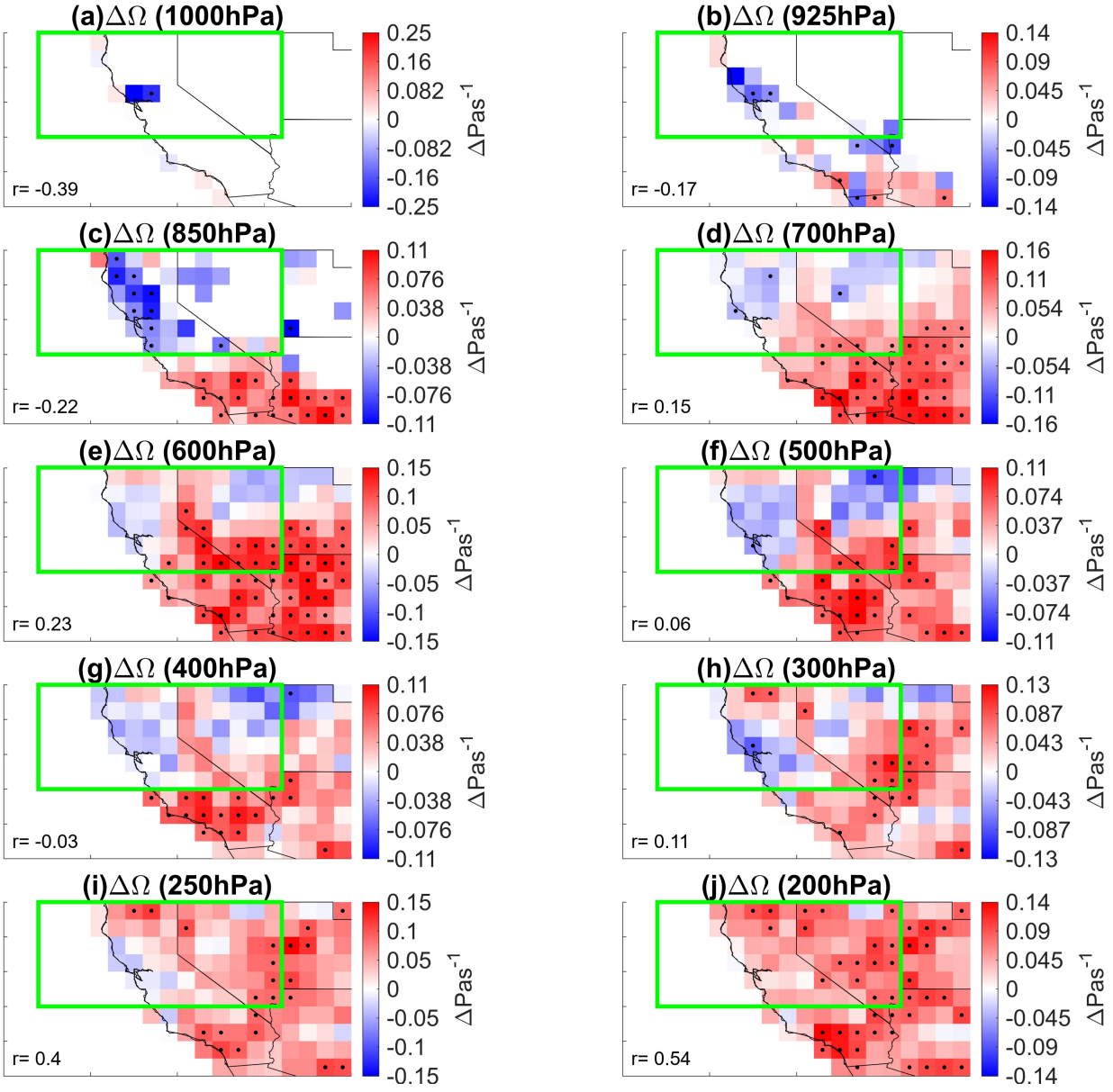

Figure S15. High minus low DM days' MERRA-2 Ω anomalies at all AIRS pressure levels from 1000 hPa to 200 hPa (a-j) under high RH_s conditions in the 2003-2022 June-October time period. Black dots indicate statistical significance at the 90% confidence interval. r values indicate spatial Pearson cross correlations between total Ω and MODIS AOD.

References

Global Modeling And Assimilation Office and Pawson, S.: MERRA-2 inst3_3d_aer_Nv: 3d,3-Hourly,Instantaneous,Model-Level,Assimilation,Aerosol Mixing Ratio V5.12.4, https://doi.org/10.5067/LTVB4GPCOTK2, 2015.

Keeley, J. E. and Syphard, A. D.: Twenty-first century California, USA, wildfires: fuel-dominated vs. wind-dominated fires, Fire Ecology, 15, 24, https://doi.org/10.1186/s42408-019-0041-0, 2019.

Omar, A. H., Winker, D. M., Vaughan, M. A., Hu, Y., Trepte, C. R., Ferrare, R. A., Lee, K.-P., Hostetler, C. A., Kittaka, C., Rogers, R. R., Kuehn, R. E., and Liu, Z.: The CALIPSO Automated Aerosol Classification and Lidar Ratio Selection Algorithm, Journal of Atmospheric and Oceanic Technology, 26, 1994–2014, https://doi.org/10.1175/2009JTECHA1231.1, 2009.

Tackett, J. L., Winker, D. M., Getzewich, B. J., Vaughan, M. A., Young, S. A., and Kar, J.: CALIPSO lidar level 3 aerosol profile product: version 3 algorithm design, Atmospheric Measurement Techniques, 11, 4129–4152, https://doi.org/10.5194/amt-11-4129-2018, 2018.

Winker, D.: CALIPSO Lidar Level 3 Tropospheric Aerosol Profiles, All Sky Data, Standard V4-20, https://doi.org/10.5067/CALIOP/CALIPSO/CAL_LID_L3_TROPOSPHERIC_APRO_ALLSKY-STANDARD-V4-20, 2019.